Journal of Magnetic Resonance 252 (2015) 10–19

Contents lists available at ScienceDirect

Journal of Magnetic Resonance

journal homepage: www.elsevier.com/locate/jmr

Specific ^{13}C labeling of leucine, valine and isoleucine methyl groups for unambiguous detection of long-range restraints in protein solid-state NMR studies

Hannes Klaus Fasshuber [a,b,1], Jean-Philippe Demers [a,b,1], Veniamin Chevelkov [a,b], Karin Giller [a], Stefan Becker [a], Adam Lange [a,b,c,*]

[a] Department of NMR-based Structural Biology, Max Planck Institute for Biophysical Chemistry, Am Fassberg 11, 37077 Göttingen, Germany
[b] Department of Molecular Biophysics, Leibniz-Institut für Molekulare Pharmakologie (FMP), Robert-Rössle-Str. 10, 13125 Berlin, Germany
[c] Institut für Biologie, Humboldt-Universität zu Berlin, Invalidenstr. 110, 10115 Berlin, Germany

ARTICLE INFO

Article history:
Received 30 October 2014
Revised 10 December 2014
Available online 6 January 2015

Keywords:
Nuclear Magnetic Resonance
Solid-state NMR
α-Ketoisovalerate
α-Ketobutyrate
^{13}C methyl labeling
Protein structure
Distance restraints
Proton detection
Dynamics

ABSTRACT

Here we present an isotopic labeling strategy to easily obtain unambiguous long-range distance restraints in protein solid-state NMR studies. The method is based on the inclusion of two biosynthetic precursors in the bacterial growth medium, α-ketoisovalerate and α-ketobutyrate, leading to the production of leucine, valine and isoleucine residues that are exclusively ^{13}C labeled on methyl groups. The resulting spectral simplification facilitates the collection of distance restraints, the verification of carbon chemical shift assignments and the measurement of methyl group dynamics. This approach is demonstrated on the type-three secretion system needle of *Shigella flexneri*, where 49 methyl–methyl and methyl–nitrogen distance restraints including 10 unambiguous long-range distance restraints could be collected. By combining this labeling scheme with ultra-fast MAS and proton detection, the assignment of methyl proton chemical shifts was achieved.

1. Introduction

Solid-state NMR (ssNMR) is a powerful analytical technique which provides site-specific information on the local molecular structure of complex biological systems. It is capable of investigating challenging samples: high molecular weight, insoluble and non-crystalline systems. Biomaterials which have been studied by ssNMR include amyloid fibrils [1–4], membrane proteins [5–7], virus capsids [8,9], bacterial filamentous proteins [10,11], fibrillar proteins such as collagen, keratin and silk [12,13] and bone and teeth mineral materials [14]. Solid-state NMR studies of large systems are however technically challenging due in part to the high crowding of spectra, in addition to the intrinsically low sensitivity and broad line-width of NMR resonances in the solid state. New techniques have been recently introduced to improve the resolution and sensitivity of magic-angle spinning (MAS) ssNMR spectra, including the use of high external magnetic fields, novel pulse sequence implementations for the observation of long-range distance correlations, an increase in the magic-angle spinning rates [15], proton detection and the introduction of various isotopic labeling strategies (see below). Major steps in structural studies of biomolecules by ssNMR are the assignment of chemical shifts for various nuclei, the collection of structural restraints such as long-range distance restraints, and the study of local dynamics. Here we present a strategy for the isotopic ^{13}C labeling of leucine, valine and isoleucine methyl groups and demonstrate how this labeling scheme facilitates the collection of distance restraints, the verification of carbon chemical shift assignments and the measurement of methyl group dynamics. We combined this labeling scheme with ultra-fast MAS ($\geqslant$60 kHz MAS) and proton detection in order to obtain the chemical shift assignments of methyl protons.

Solid-state NMR spectra recorded on uniformly-labeled samples contain a large number of carbon resonances which have broad line-widths due to one-bond dipolar and scalar ^{13}C–^{13}C homonuclear couplings. Both factors contribute to low spectral resolution

* Corresponding author at: Department of Molecular Biophysics, Leibniz-Institut für Molekulare Pharmakologie (FMP), Robert-Rössle-Str. 10, 13125 Berlin, Germany. Fax: +49 30 94793 109.
E-mail address: alange@fmp-berlin.de (A. Lange).
[1] These authors contributed equally to this work.

http://dx.doi.org/10.1016/j.jmr.2014.12.013
1090-7807/

and high ambiguity of cross-peaks. Uniformly-labeled samples present further disadvantages for the collection of long-range restraints: as the initial signal is shared among a large number of ^{13}C labeled nuclei, the intensity of cross-peaks is reduced; as well, the presence of strong dipolar truncation in uniformly labeled samples suppresses the transfer of magnetization between weakly coupled nuclei, hindering the detection of long-range distances.

In the past, different approaches have been presented to obtain structural information on uniformly-labeled samples. One such approach is the development of new pulse sequences to collect long-range distance restraints: (1) CHHC and NHHC for proton–proton distances [16,17]; (2) third-spin assisted sequences: PDSD [18,19], RAD/DARR [20,21] and PAR [22] for carbon–carbon distances; (3) PAIN [23] for heteronuclear correlations such as ^{13}C–^{15}N. Alternatively, REDOR [24] and TEDOR [25] are first-order dipolar recoupling experiments suited to measure heteronuclear distances, respectively.

Former solutions to the dipolar truncation problem also exploit sparse ^{13}C labeling schemes, in which different ^{13}C labeled precursors act as the sole ^{13}C source in the growth medium during bacterial expression of the protein. Sparsely ^{13}C labeled protein samples present in addition to the reduction of dipolar truncation two advantages: first, spectra are simplified since a smaller number of ^{13}C atoms are labeled in the protein; second, the resolution of ^{13}C peaks is increased due to the removal of one-bond dipolar and scalar ^{13}C–^{13}C couplings. Both result in a strong reduction of cross-peak overlap in ssNMR spectra, leading to a simpler determination of unambiguous long-range distances restraints. Examples of sparse labeling schemes used in ssNMR comprise [1,3-^{13}C]-glycerol (Glyc) and [2-^{13}C]Glyc [26–29], [1-^{13}C]-glucose [30] (Glc), [2-^{13}C]Glc [31,32], [1-^{13}C]-acetate [33] and various ^{13}C labeled pyruvates [34]. Long-range distance restraints are obtained in combination with sparse labeling by recording ssNMR experiments suited for the observation of long-range distances as previously mentioned, or also with ^{13}C–^{13}C first-order dipolar recoupling sequences such as RFDR [35,36] as demonstrated using [2-^{13}C]Glyc labeling [37]. Significant improvements in the resolution of ^{13}C–^{13}C ssNMR spectra have been demonstrated by using [1-^{13}C]Glc and [2-^{13}C]Glc sparsely-labeled proteins [38,39]. With these labeling schemes, a strategy was presented to determine intermolecular interactions of proteins in a self-assembled molecular system [31]. Additionally, the [2-^{13}C]Glc labeling allows the easy stereospecific assignment for the amino acids valine and leucine [40] and can be used for the recording of long-range distance restraints in 3D spectra [41].

Previous studies exhibit the prevalent application of sparsely labeled methyl groups to gain structural, functional and dynamics information of proteins [42–45]. In addition, unambiguous long-range correlations between methyl groups are important as methyl groups tend to be found deep in the hydrophobic core of proteins. However, a drawback of the glycerol and glucose labeling schemes lies in the high spectral crowding of the methyl ^{13}C region. Many amino acids containing methyl groups – threonine, alanine, valine, isoleucine, leucine and methionine – often have their methyl groups concurrently labeled in [1,3-^{13}C]Glyc and [1-^{13}C]Glc labeling schemes, maintaining a strong ambiguity of cross-peaks in ^{13}C ssNMR spectra.

We propose to resolve this problem by utilizing the biosynthetic precursors α-ketoisovalerate, similar to recent investigations by Huber et al. [46], and α-ketobutyrate [47]. In contrast to previous studies we are investigating protonated rather than deuterated protein samples and focus on carbon–carbon distance restraints which would be difficult to obtain with deuterated proteins under ultra-fast spinning conditions. Considering the biosynthetic metabolism of amino acids (Fig. 1), one obtains only ^{13}C labeled methyl groups on leucine and valine when using labeled α-ketoisovalerate. The Cδ1 methyl group of isoleucine can be ^{13}C labeled by using labeled α-ketobutyrate. This leads to an improvement of the information content obtained from the methyl–methyl region of ^{13}C–^{13}C 2D spectra as the ambiguity of methyl–methyl cross-peaks is largely reduced. This benefit facilitates collecting unambiguous distance restraints between carbons of methyl groups that are close in space. Here, we demonstrate the detection of long-range restraints in the type-three secretion system (T3SS) needle of *Shigella flexneri*. We also analyze the intensity of intra-residue cross-peaks and the relaxation properties of methyl carbons. Employing ultra-fast MAS rates and sparse ^{13}C labeling of methyl groups, we also obtain high-resolution proton-detected ^{13}C–^{1}H correlations yielding the assignment of methyl protons.

2. Material and methods

2.1. Sample preparation

MxiH proteins were expressed recombinantly in *Escherichia coli* strain BL21(DE3) in minimal medium during 5 h. For the production of the [LV-^{13}C methyl]-labeled sample, sodium α-ketoisovalerate [2-keto-3-(methyl-^{13}C)-butyric acid-4-^{13}C sodium] (125 mg/L) was added as carbon source one hour prior to induction. For the [U-^{15}N, ILV-^{13}C methyl]-labeled sample, $^{15}NH_4Cl$ was used as nitrogen source. One hour before induction, sodium α-ketoisovalerate [2-keto-3-(methyl-^{13}C)-butyric acid-4-^{13}C sodium] (125 mg/L) and sodium α-ketobutyrate [2-Ketobutyric acid-4-^{13}C sodium] (125 mg/L) were added as carbon source. Both proteins were purified by following the protocol established for *Salmonella typhimurium* PrgI needles [38]. The N-terminal hepta-Histidine (His) tag was cleaved using tobacco etch virus protease, releasing MxiH proteins containing the non-native N-terminal residues glycine and histidine. The protein concentration was raised to 0.2 mM during polymerization, which took place at 37 °C for 16 days and approximately 20 mg of needles were produced.

2.2. Solid-state NMR

MxiH needles were ultra-centrifuged and transferred into a 4.0-mm and a 1.3-mm ZrO_2 ssNMR rotor. Solid-state NMR experiments for the [LV-^{13}C methyl] and the [U-^{15}N, ILV-^{13}C methyl]-labeled samples were recorded on an 18.8-Tesla spectrometer (Bruker Biospin, Germany). The [U–^{13}C]Glc-labeled and [2-^{13}C]Glc-labeled spectra were conducted on a 20-Tesla spectrometer (Bruker Biospin, Germany). Carbon-detected experiments were conducted at 11 kHz MAS frequency (4.0-mm rotor) and a temperature of 7.5 °C, while in proton-detected experiments the sample was spun at 60 kHz MAS frequency (1.3-mm rotor) and had an effective sample temperature of +35 °C. Proton-detected experiments were conducted only the [U-^{15}N, ILV-^{13}C methyl]-labeled sample. The temperature was calibrated via the ^{1}H chemical shift of water in reference to DSS [48].

All spectra were processed using Bruker Topspin 3.1. For 2D and 3D spectra, the free induction decay (FID) signals were apodized prior to Fourier transform, using sine squared window functions: the sine bell shift was 45° for all carbon-detected spectra, respectively 43° and 47° for the ^{1}H and ^{13}C dimensions of the 2D (H)CH spectrum (Fig. 7a) and 47° for all dimensions of the 3D (H)CCH spectrum (Fig. 7b). The chemical shift assignment of spectra was carried out using the Sparky software [49].

2.3. Carbon-detected solid-state NMR

The 1D CP spectra (Fig. 2a and b, Fig. 4a) were acquired with the following parameters: maximal acquisition time AQ = 50 ms, recy-

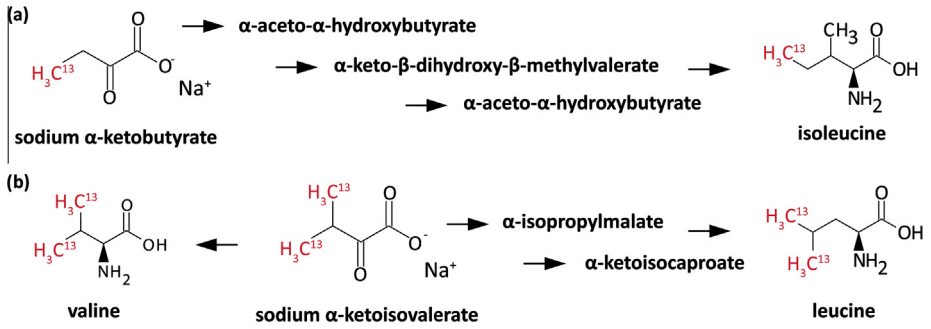

Fig. 1. Biosynthetic labeling patterns of the residues isoleucine, leucine and valine based on the provided precursors (a) sodium α-ketobutyrate resulting in ^{13}Cδ1-labeled isoleucine and (b) sodium α-ketoisovalerate resulting in ^{13}Cγ1,^{13}Cγ2-labeled valine and ^{13}Cδ1,^{13}Cδ2-labeled leucine.

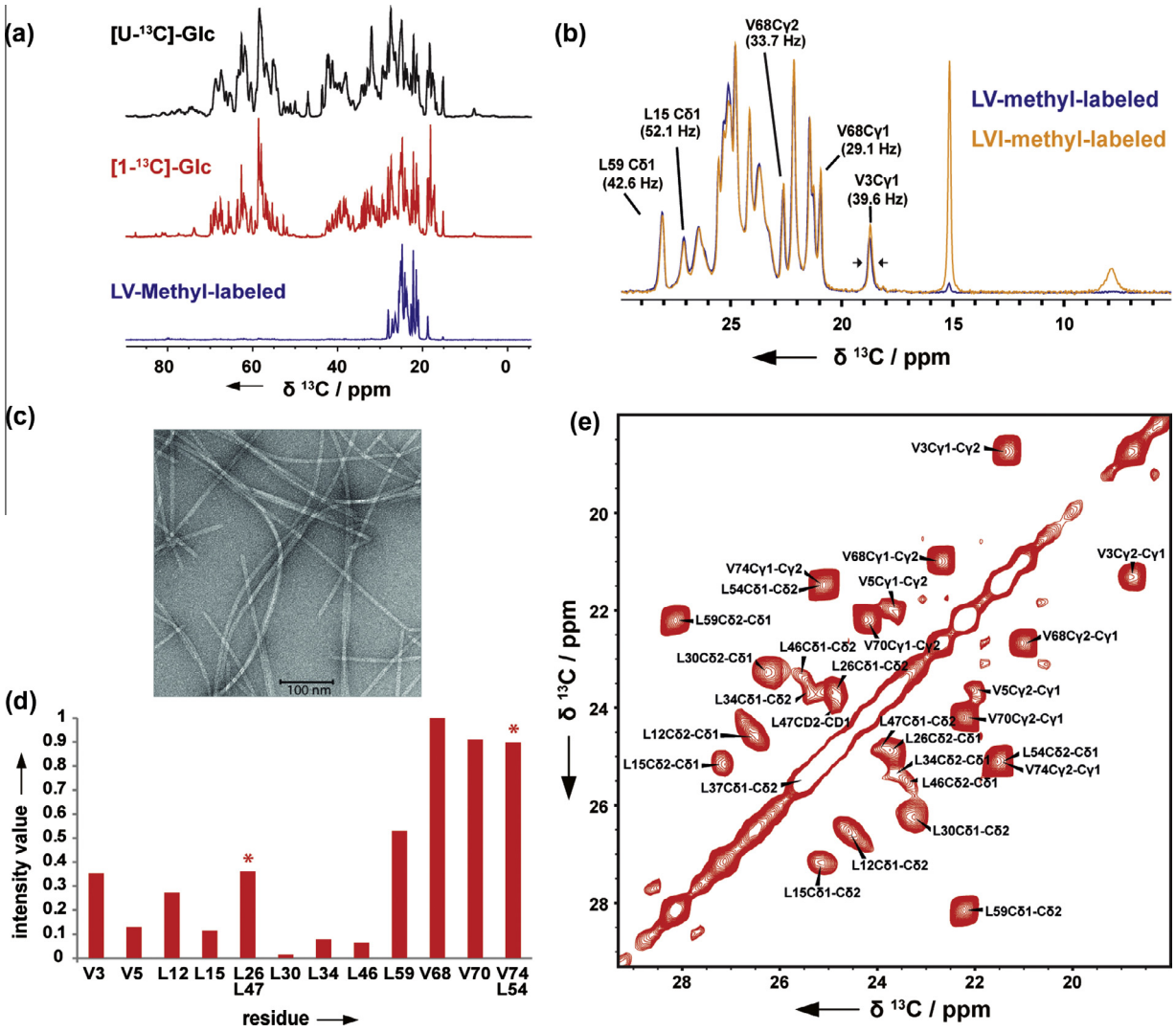

Fig. 2. (a) Excerpts of 1D CP spectra of (black) [U-^{13}C]Glc-, (red) [1-^{13}C]Glc- and (violet) [LV-^{13}C methyl]-labeled MxiH needles. (b) Comparison of the [LV-^{13}C methyl]-labeled sample (blue) with the [U-^{15}N, ILV-^{13}C methyl]-labeled sample (yellow; with full line widths at half-height (FWHH) indicated for isolated resonances). (c) Electron microscopy image of T3SS MxiH needles used in this study. (d) Intensities of intra-residue cross-peaks obtained from the 2D PDSD spectrum of the [LV-^{13}C methyl]-labeled sample presented in (e). Asterisks indicate overlapping cross-peaks, see residues listed at the bottom. (e) 2D PDSD spectrum of [LV-^{13}C methyl]-labeled MxiH needles recorded with a mixing time of 50 ms. The cross-peak L37 Cδ1/Cδ2, located on the diagonal, was confirmed by a ^{13}C–^{13}C double-quantum single-quantum (DQ–SQ) spectrum recorded on the uniformly-labeled sample [39]. The 2D spectrum was recorded on an 800 MHz spectrometer at 11 kHz MAS frequency. (For interpretation of the references to color in this figure legend, the reader is referred to the web version of this article.)

cling delay (RD) of 5 s. No window function was applied in the processing. The build-up of ^{15}N magnetization transferred during ^{15}N–^{13}C SPECIFIC-CP [50,51] was determined in a series of 1D experiments (Fig. 6b) where the contact time of the ^{15}N–^{13}C CP was varied from 5 ms up to 15 ms in steps of 2.5 ms. The experiments were recorded using the following parameters: AQ = 10 ms, RD of 2.5 s and a number of scans (NS) of 5120. The nutation frequencies employed during the ^{15}N–^{13}C CP transfer were 8.8 kHz

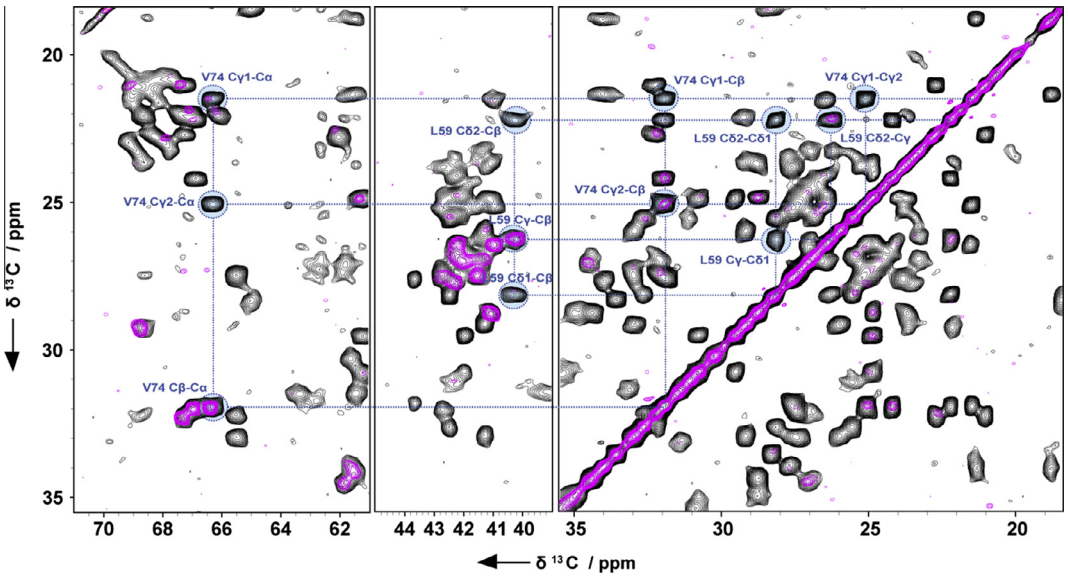

Fig. 3. 2D PDSD spectra of [U-^{13}C]Glc- (in black) and [2-^{13}C]Glc-labeled (in magenta) T3SS MxiH needles, recorded with a PDSD mixing time of 50 ms. Spin system correlations of V74, L59 are highlighted in blue. The stereospecific assignment for the methyl carbons of valine and leucine can be identified using the appearance of Cβ–Cδ1 and Cγ–Cδ2 cross-peaks in leucine, and Cα–Cγ1 and Cα–Cγ2 in valine, following the method introduced in Ref. [40]. The experiments were conducted on an 850 MHz spectrometer at 11 kHz MAS frequency. (For interpretation of the references to color in this figure legend, the reader is referred to the web version of this article.)

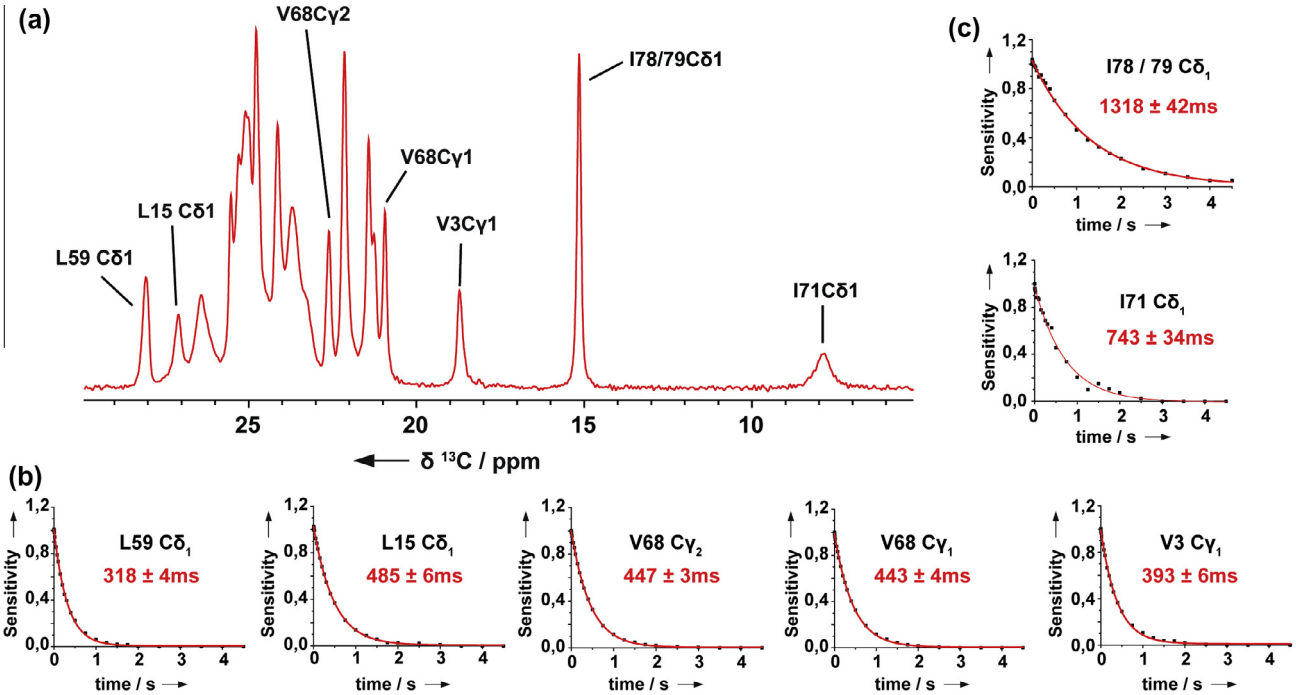

Fig. 4. (a) 1D CP spectrum of [U-^{15}N, ILV-^{13}C methyl]-labeled sample. (b) ^{13}C T_1 relaxation curves of leucine and valine methyl groups that can be unambiguously assigned in the 1D spectrum. (c) ^{13}C T_1 relaxation curves for isoleucine methyl groups. For (b) and (c), the apparent ^{13}C T_1 relaxation times calculated from fitting are indicated in red (Avg. ± SD). The spectra were acquired on an 800 MHz spectrometer at 11 kHz MAS frequency. (For interpretation of the references to colour in this figure legend, the reader is referred to the web version of this article.)

RF on the ^{13}C channel, 4.5 kHz RF on the ^{15}N channel and 58 kHz RF on the ^{1}H channel.

For the [LV-^{13}C methyl]-labeled sample, two 2D PDSD spectra were acquired (Figs. 2e and 5a), with PDSD mixing times of 50 ms or 800 ms, using the following parameters: AQ_1 = 12 ms (indirect dimension), AQ_2 = 15 ms (direct dimension), spectral window SW_1 = 22 ppm (indirect dimension), SW_2 = 346 ppm (direct dimension), RD of 3 s, CP contact time of 0.8 ms, NS = 256 (for PDSD 50 ms) or NS = 1856 (for PDSD 800 ms), for total experimental times of 23 h (for PDSD 50 ms) and 6 days 19 h (for PDSD 800 ms). For the [U-^{15}N, ILV-^{13}C methyl]-labeled sample, a PDSD spectrum with mixing time of 800 ms was recorded (Fig. 5a) using the following parameters: AQ_1 = 12 ms (indirect dimension), AQ_2 = 15 ms (direct dimension), spectral window SW_1 = 80 ppm (indirect dimension), SW_2 = 345 ppm (direct dimension), RD of 3 s, CP contact time of 0.5 ms, NS = 320, for a total experimental time of 5 days 11 h. The spectrum of the [U-^{13}C]Glc-labeled sample (Fig. 3) was recorded with a PDSD mixing time of 50 ms, using

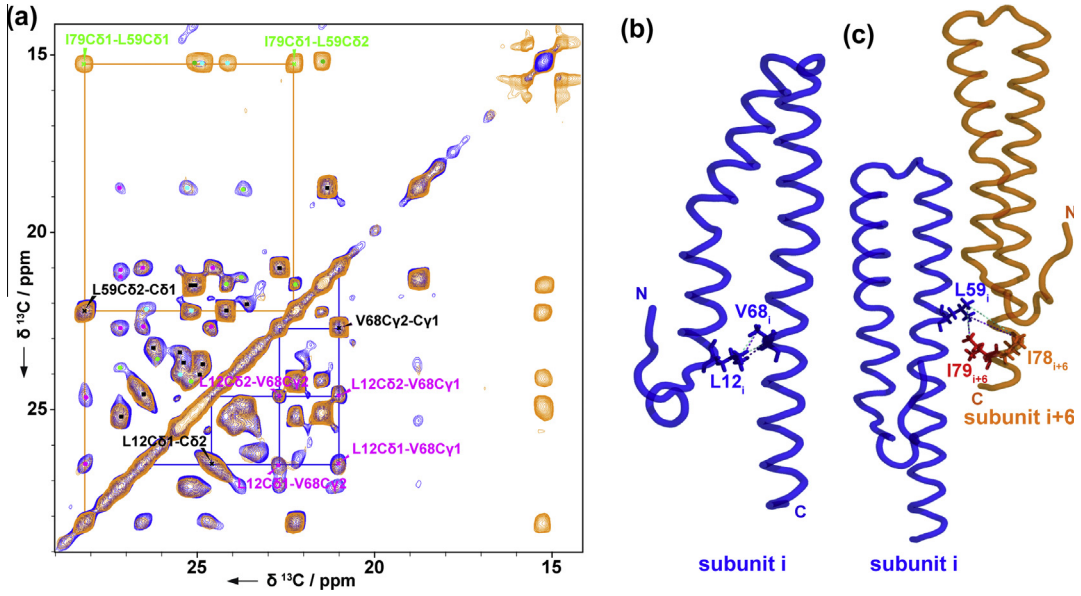

Fig. 5. (a) Comparison of the [LV-^{13}C methyl]-labeled sample (blue) and the [U-^{15}N, ILV-^{13}C methyl]-labeled sample (yellow). PDSD-spectra were recorded with a mixing time of 800 ms. The labels and cross-peak marks which are colored in black represent intra-residual interactions, in magenta unambiguous distance restraints and in green structurally unambiguous distance restraints. The up-field shifted Cδ1 resonance of isoleucine I71 (at 8.0 ppm) is not shown. (b) The unambiguous distance restraints between L12 and V68, identified in the 2D PDSD spectrum of the [LV-^{13}C methyl]-labeled sample, are illustrated on the atomic structure of MxiH needles from Ref. [63]. (c) Representation of the structurally unambiguous distance restraints between L59 and I79Cδ1, as observed in the 2D PDSD spectrum of the [U-^{15}N, ILV-^{13}C methyl]-labeled sample. The spectra were measured on an 800 MHz spectrometer at 11 kHz MAS frequency. (For interpretation of the references to color in this figure legend, the reader is referred to the web version of this article.)

maximum acquisition times of 19 ms (direct dimension) and 15 ms (indirect dimension). The total experimental time was 1 day 17 h. The spectrum of the [2-^{13}C]Glc-labeled sample (Fig. 3) was recorded with a PDSD mixing time of 50 ms, using maximum acquisition times of 21 ms (direct dimension) and 15 ms (indirect dimension). The total experimental time was 1 day 7 h.

The NCX spectrum (Fig. 6a) was recorded on the [U-^{15}N, ILV-^{13}C methyl]-labeled sample with AQ_1 = 10 ms (indirect dimension), AQ_2 = 10 ms (direct dimension), spectral window SW_1 = 39.8 ppm (indirect dimension), SW_2 = 282 ppm (direct dimension), RD of 3.7 s, initial ^{1}H–^{15}N CP contact time of 1400 μs. The ^{15}N–^{13}C SPECIFIC CP [50,51] transfer was achieved using a contact time of 12 ms with a decoupling of 58 kHz RF on ^{1}H, a number of scans NS = 1408, for a total experimental time of 3 days 21 h.

The apparent ^{13}C longitudinal relaxation times T_1 were measured on the [U-^{15}N, ILV-^{13}C methyl]-labeled sample in 1D ^{13}C experiments (Fig. 4b and c). Following initial cross-polarization to ^{13}C, carbon magnetization was placed along the longitudinal axis during a variable relaxation delay, then brought back to the transverse plane for detection. The relaxation delay was set in the range from 1 μs to 4.5 s. Experiments were recorded with AQ = 30 ms, NS = 256, RD of 10 s and a total experimental time for all experiments of 21 h.

2.4. Proton-detected solid-state NMR

The proton-detected 2D ^{13}C–^{1}H heteronuclear correlation spectrum (Fig. 7a) was recorded according to the conventional (H)CH pulse sequence [52] presented in Supplementary Fig. S4A. The acquisition times for the direct and indirect dimensions were 8 ms and 40.7 ms, respectively. In the 3D (H)CCH experiment (Supplementary Fig. S4B), ^{13}C–^{13}C homonuclear dipolar interactions were recoupled by RFDR [35,36], thus yielding information about carbon–carbon contacts. Maximal acquisition times were AQ_1 = 22.6 ms, AQ_2 = 16.8 ms (indirect dimensions) and AQ_3 = 7 ms (direct dimension). RFDR-16 recoupling was applied during 19.2 ms and the applied carbon RF field was 45 kHz. In all the experiments during ^{1}H–^{13}C CP, the carbon RF field was ramped down from 100% to 70% with an average value of 15 kHz, while the proton RF field was kept constant at 45 kHz. The CP contact times were 520 μs and 320 μs for ^{1}H–^{13}C and ^{13}C–^{1}H transfer, respectively. During ^{13}C evolution, ^{1}H–^{13}C couplings were removed by application of low-power XiX [53] on the proton channel with an RF strength of 12 kHz. During proton detection, the ^{1}H–^{13}C scalar couplings were removed using WALTZ-16 decoupling [54] with an RF strength of 7 kHz. The experiment times were 20.5 h and 4 days 12 h for the 2D and 3D experiment, respectively.

3. Results and discussion

3.1. Isotopic labeling pattern

The knowledge of the biosynthetic pathways of amino acids (Fig. 1) allows prediction of the labeling pattern which can be achieved in proteins expressed in *E. coli* [55]. To identify the labeling pattern obtained in our approach, we recorded solid-state NMR experiments on assembled MxiH needles. Two MxiH needle samples were produced: first, an [LV-^{13}C methyl]-labeled sample was prepared using the sodium α-ketoisovalerate precursor ^{13}C labeled at both methyl groups; second, a [U-^{15}N, ILV-^{13}C methyl]-labeled sample was produced using three labeled precursors: sodium α-ketoisovalerate and sodium α-ketobutyrate [56,57] ^{13}C labeled at the methyl groups and $^{15}NH_4Cl$.

Solid-state NMR 1D cross-polarization (CP) spectra were recorded for these samples and compared to spectra obtained from two established ^{13}C labeling strategies [39]: uniform labeling [U-^{13}C]Glc, and sparse labeling [1-^{13}C]Glc (Fig. 2a). As previously demonstrated, the [1-^{13}C]Glc- and [2-^{13}C]Glc-labeled spectra show a large improvement in ^{13}C resolution and line-widths relative to [U-^{13}C]Glc-labeled spectra, due to the removal of a majority of one-bond ^{13}C–^{13}C dipolar and *J* couplings [32]. However, 2D ^{13}C–^{13}C correlation spectra are highly crowded in the chemical

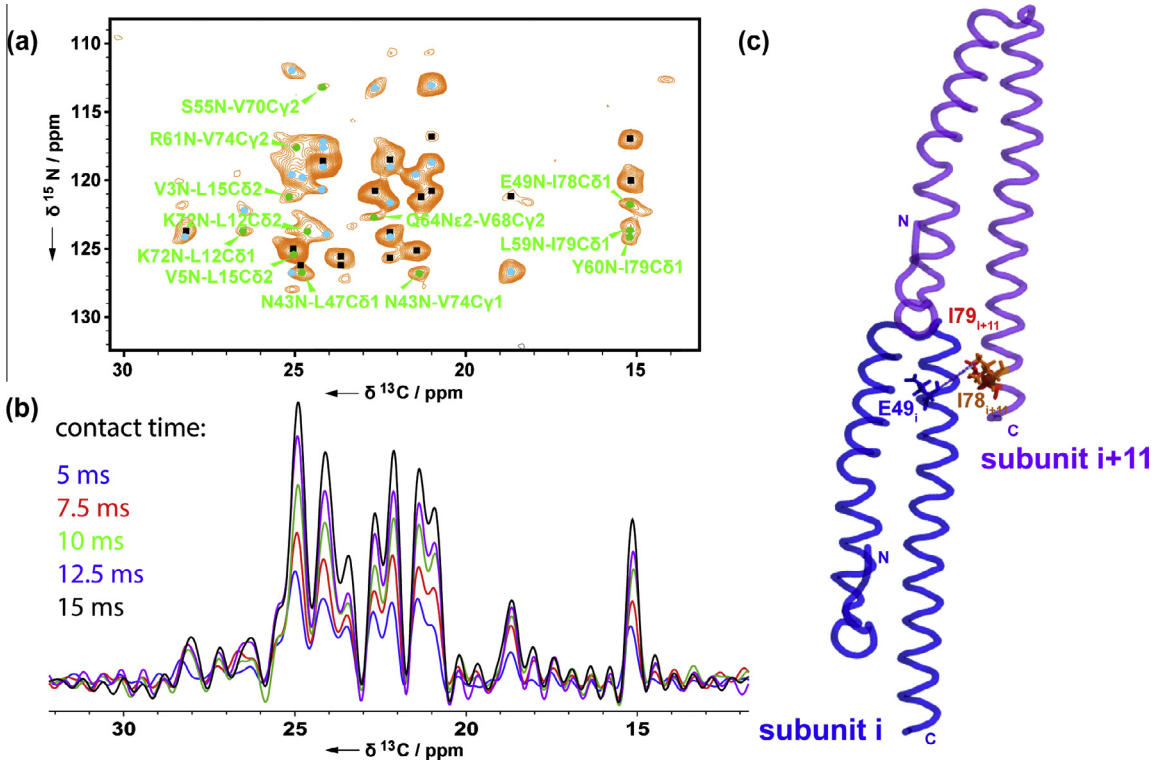

Fig. 6. (a) 2D NCX correlation spectrum of the [U-^{15}N, ILV-^{13}C methyl]-labeled MxiH needle sample with structurally unambiguous distance restraints highlighted in green. The cross peaks which are colored in black represent intra residual correlations, the ones in blue and green ambiguous and structurally unambiguous correlations. (b) 1D NCX spectra as a function of SPECIFIC-CP contact time in the range from 5 to 15 ms. Both 2D and 1D spectra were recorded on an 800 MHz spectrometer at 11 kHz MAS frequency. (c) Illustration of the structurally unambiguous distance restraint between E49N and I78Cδ1, observed in the 2D NCX spectrum, represented on the atomic structure of MxiH needles from Ref. [63]. (For interpretation of the references to color in this figure legend, the reader is referred to the web version of this article.)

shift range from 15 ppm to 30 ppm which corresponds to the methyl region of amino acids since methyl carbons can be ^{13}C labeled for all amino acid types in the [1-^{13}C]Glc labeling scheme. For some amino acids, carbon resonances from CH_2 groups can also be found in the same chemical shift range as methyl groups. In contrast, the [LV-^{13}C methyl]-labeled MxiH spectrum shows only signals from leucine and valine methyl carbons, in the chemical shift range from 15 ppm to 28 ppm (shown in Fig. 2a; see also Supplementary Figs. S1 and S2).

The comparison between the [U-^{15}N, ILV-^{13}C methyl]-labeled sample with the [LV-^{13}C methyl]-labeled sample demonstrates the similarity of the valine and leucine methyl resonances both in resolution and signal intensity as well as the addition of the Cδ1 methyl carbons of isoleucines in the [U-^{15}N, ILV-^{13}C methyl]-labeled sample (Fig. 2b), which are essentially absent from the [LV-^{13}C methyl] spectrum. No significant signals were detected in other regions of the 1D CP spectra, demonstrating the absence of scrambling (i.e. undesired biosynthetic pathways) in the labeling patterns. This was further confirmed by recording 2D PDSD spectra with short mixing time (50 ms PDSD, Fig. 2e) for both the LV- and ILV-labeled samples. Cross-peaks only appear where predicted according to the published chemical shifts [39] (see Supplementary Table S1 and BMRB entry 18651).

A remarkable advantage of the ^{13}C methyl labeling strategies is that the high resolution obtained in [1-^{13}C]Glc- and [2-^{13}C]Glc-labeled samples is conserved (Supplementary Fig. S1), due to the absence of neighboring ^{13}C labeled nuclei. Indeed, the carbon resonances are very sharp, with line-widths measured on isolated resonances ranging from 29.1 Hz (0.14 ppm) to 52.1 Hz (0.26 ppm) (Fig. 2b).

The prochiral methyl carbons of leucine and valine residues were stereospecifically assigned by means of the [2-^{13}C]Glc labeling strategy as previously introduced [40]. The stereospecific assignment of valine residues was obtained based on the presence of cross-peaks for Cα–Cγ1 and Cβ–Cγ2 as illustrated with the assignment of V74Cγ1 and V74Cγ2 (Fig. 3). For leucine residues, the unambiguous assignment of the prochiral methyl groups is extracted from the presence of cross-peaks in ^{13}C–^{13}C correlation spectra for Cβ–Cδ1 and Cγ–Cδ2, shown in Fig. 3 for the spin system of L59. The stereospecific assignment of methyl groups is structurally relevant since side-chain rotamer conformations can be identified from the methyl ^{13}C chemical shifts [58].

3.2. Dynamics in the MxiH needle

Next, we analyzed line widths and relaxation of the Leu, Val and Ile methyl groups. We observed strong differences in the signal intensities of intra-residue cross-peaks (Fig. 2d) measured from the short mixing time 2D PDSD spectrum (Fig. 2e). Peaks corresponding to amino acids located in the C-terminal helix of the MxiH needle were more intense. The C-terminal helices, lining the inside lumen of the needle assembly [38,39], may be more tightly packed than the N-terminal helices present at the outer surface of the needle. Similar differences in cross-peak intensities were also observed in a DNP study of MxiH needles [59]. Among different bacterial species, it was observed that the amino acid sequence of the T3SS needle protein is more conserved in this C-terminal helix [39].

We also measured the apparent ^{13}C T_1 relaxation times of Leu, Val and Ile methyl groups in MxiH, as knowledge of this parameter is highly valuable to choose appropriate mixing times in PDSD experiments for recording distances restraints. Due to the highly resolved carbon resonances in the 1D CP spectrum of [U-^{15}N, ILV-^{13}C methyl]-labeled MxiH (Fig. 4a), we are able to select six isolated methyl peaks. The apparent ^{13}C T_1 relaxation times mea-

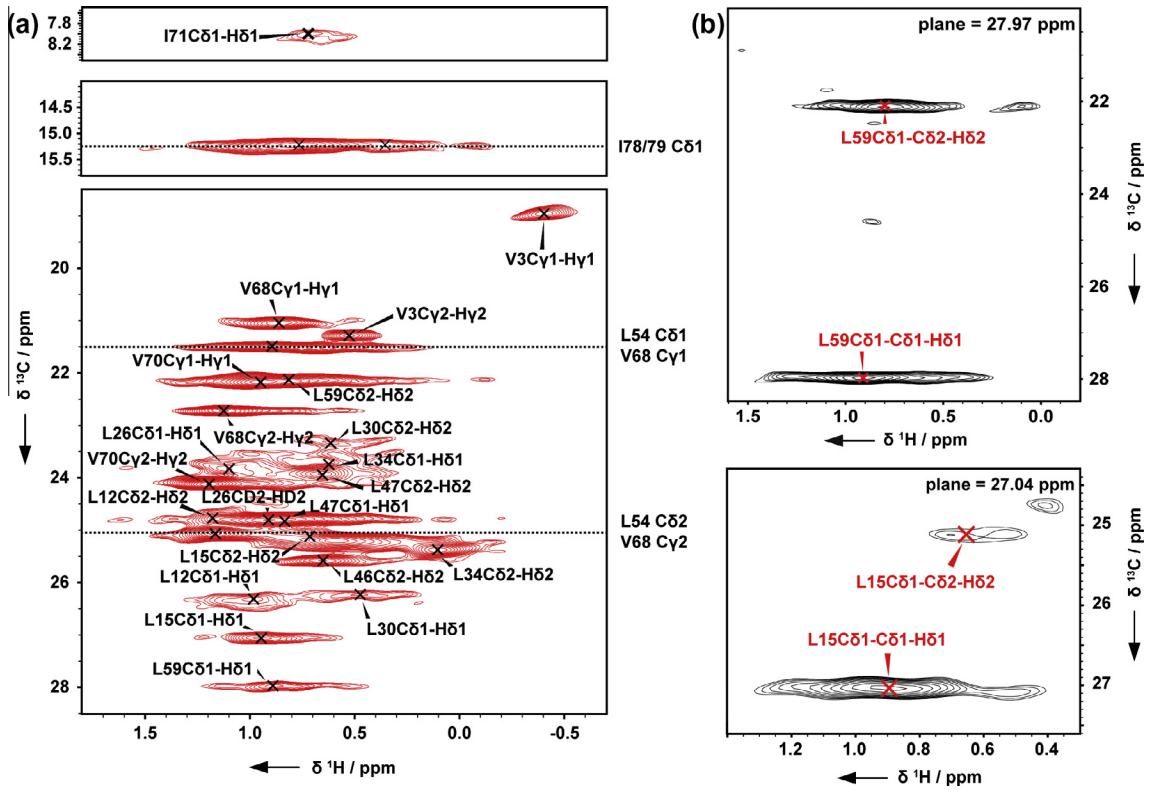

Fig. 7. (a) Two dimensional proton-detected (H)CH correlation spectrum. Three dashed lines show unresolved signals originating from known resonances, which are indicated on the right side of the panel. (b) Two representative planes from a 3D (H)CCH correlation spectrum illustrate the assignment of methyl protons from the same amino acid. Carbon isotropic chemical shift values in the indirect dimension are indicated. The spectra were conducted on an 800 MHz spectrometer at a 60 kHz MAS frequency.

sured at 11 kHz MAS on an 800 MHz spectrometer range from 318 ms to 485 ms for leucine and valine residues.

The isoleucine resonances show a longer apparent T_1: the I71Cδ1 resonance exhibits a T_1 value of 743 ms; the isoleucine I78 and I79 resonances overlap; however, the fitted curve corresponds to a T_1 value of 1.32 s (Fig. 4c). Although the values for T_1 differ between residues, a structural interpretation of the T_1 values is difficult due to the strong influence of carbon–carbon spin diffusion during the measurements at 11 kHz MAS. Ultra-fast MAS rates ($\geqslant$60 kHz) would be required to suppress this effect. For the observation of long-range distance cross-peaks, PDSD mixing times longer than 400 ms are usually employed to allow sufficient transfer of magnetization. However, the inspection of the ^{13}C T_1 decay curves for leucine and valine residues reveal that mixing times longer than 1 s would result in a reduction of the magnetization amount to 10% of its initial level. We can suggest PDSD mixing times in the range of 400–800 ms for the observation of long-range distance correlations corresponding to a decay of 40–20 %. Although some mixing schemes such as RAD/DARR [20,21] provide faster magnetization transfer, we employed the PDSD mixing scheme [18,19] for the recording of all correlation spectra. In PDSD, no RF irradiation is applied, increasing the safety of the probehead.

3.3. ^{13}C–^{13}C distance restraints

In order to collect long-range distance restraints, we recorded 2D spectra with a long PDSD mixing time of 800 ms for both the [LV-^{13}C methyl]- and [U-^{15}N, ILV-^{13}C methyl]-labeled sample (Fig. 5a). By comparing those spectra with short PDSD mixing time spectra (Fig. 2e), multiple long-range cross-peaks can be observed. A long-range correlation is defined to be between residue i and j where $[|i-j| \geqslant 5]$. In our analysis, we picked all peaks in the spectrum and excluded all short-range $[1 \leqslant |i-j| \leqslant 2]$ correlations.

The long-range cross-peaks were classified as frequency unambiguous (also known as spectrally unambiguous), structurally unambiguous, or ambiguous. For each cross-peak, all assignment possibilities were considered which had a chemical shift deviation of less than 0.15 ppm between the resonance frequency and the frequency present in the BMRB (BMRB entry 18651). If only one assignment possibility is present in the tolerance window, the correlation is classified as frequency unambiguous (Supplementary Table S2). The frequency unambiguous correlations define unequivocally the 3D fold of the subunit and the supramolecular subunit-subunit interfaces. As an example, all four possible methyl-methyl contacts between residues L12 and V68 are frequency unambiguous and highlighted in magenta in Fig. 5a. During the analysis of the distance restraints, some of the remaining long-range correlations can then be further assigned unambiguously by employing the 3D structure initially identified using the frequency unambiguous cross-peaks. Indeed, long-range correlations are usually assigned in an iterative procedure [60–62]. To determine the number of such structurally unambiguous correlations that can be obtained using our labeling approach, we used the atomic structure of the MxiH needle assembly recently determined on the basis of a cryo-EM density map, solid-state NMR restraints and Rosetta modelling [63].

For each long range cross-peak, we calculated the distance for every assignment possibility, including intra-molecular and inter-molecular distances. A frequency-ambiguous correlation was classified as structurally unambiguous when the shortest distance was more than 2 Å shorter than any other assignment (Supplementary Table S3). As an example, the L59 methyl carbons Cδ1 and Cδ2 have

systematically shorter distances to I79Cδ1 than to I78Cδ1, as presented in Fig. 5c. The structurally unambiguous correlations I79Cδ1–L59Cδ1 and I79Cδ1–L59Cδ2 are highlighted in green in Fig. 5a. When more than a single possibility remained, correlations were classified as ambiguous (Supplementary Table S4) and the corresponding cross-peaks are colored in blue in Fig. 5a. For this statistical analysis, the 10 lowest energy conformations of the ensemble were considered: the distances reported in Supplementary Tables S2–S4 are reported as average ± standard deviation. The ambiguous correlations can be used further in a structure calculation procedure since many software packages allow the use of ambiguous restraints [60,64]. They can also be used as independent data for validation of the structure.

From the PDSD 800 ms spectrum of the [LV-^{13}C methyl]-labeled sample (Fig. 5a), we obtained 10 frequency unambiguous correlations (Supplementary Table S2), 7 structurally unambiguous correlations (Supplementary Table S3), and 4 ambiguous correlations (Supplementary Table S4). We observe that the frequency unambiguous restraints are detected in pairs or in sets of 4 correlations (Supplementary Table 2). This redundancy corroborates the unambiguous detection of these long-range interactions. The long-range interactions between residues L12 and V68 are highlighted on the protomer structure (Fig. 5b). This information confirms the intramolecular packing of the second α-helix close to the beginning of the first α-helix of the MxiH-protein. Evaluating the spectrum of the [U-^{15}N, ILV-^{13}C methyl]-labeled sample, one can detect additional correlations between the L-V methyl carbons to the Cδ1 methyl group of I78 and I79: 4 structurally unambiguous and 4 ambiguous new correlations were found. Overall, a total of 10 unambiguous carbon–carbon distance restraints could be collected, with distances varying from 3.9 Å to 10.3 Å, and an average of 6.7 Å.

3.4. ^{15}N–^{13}C distance restraints

With $^{15}NH_4Cl$ as the sole nitrogen source in the expression medium, the recombinant proteins become uniformly ^{15}N labeled, such that ultra-sparse methyl ^{13}C labeling schemes can be used to collect N–C distance restraints by recording an NCX spectrum. In contrast to conventional ssNMR experiments such as NCA and NCO where a one-bond N–C transfer is required for the ^{15}N–^{13}C CP step, the backbone ^{15}N and methyl ^{13}C atoms are separated by three chemical bonds (valine) or four bonds (leucine, isoleucine). The intra-residual distances from the backbone ^{15}N to the ^{13}C labeled methyl carbons are larger compared to one-bond ^{15}N–^{13}C distances: on average 3.4 Å for valine, 4.3 Å for leucine and 4.4 Å for isoleucine. As a result, the contact time of the N–C transfer step has to be increased. The 1D build-up curves of the ^{15}N–^{13}C CP contact time starting from 5 ms up to 15 ms are shown in Fig. 6b. It can be seen that signals are still increasing.

A crucial element for this type of experiments is the management of the RF irradiation time. For the sake of probe safety, we have chosen a CP contact time of 12 ms with a ^{1}H decoupling strength of 58 kHz and low-power irradiation on the carbon and ^{15}N channels (8.8 kHz RF on ^{13}C, 4.5 kHz RF on ^{15}N). The 2D NCX spectrum contains intra-residue cross-peaks and sequential cross-peaks which can be used to confirm the ^{15}N and ^{13}C chemical shift assignment. Indeed, we assigned six cross-peaks for N_i to C_{i-1} correlations and one cross-peak for N_i to C_{i+1}, with distances ranging from 3.5 Å to 6.4 Å. From the 2D NCX spectrum, we also obtained a total of 12 structurally unambiguous distance restraints (Supplementary Table S3) and 8 ambiguous restraints (Supplementary Table S4). The formation of the axial interface between needle subunits i and $i + 11$ is illustrated in Fig. 6c by a structurally unambiguous contact between E49N and I78Cδ1. Distance restraints were detected with distances ranging from 5.6 Å to 12.1 Å and an average of 7.3 Å.

3.5. Proton-detected solid-state NMR

Ultra-fast MAS (⩾60 kHz MAS) and high external magnetic fields provide attractive conditions to use proton detection in fully protonated samples [15,65]. This approach provides better sensitivity compared to ^{13}C detection and improved resolution via the additional proton dimension. In addition, low-power heteronuclear decoupling schemes can be efficiently employed at ultra-fast spinning rates [53], and thus very long ^{13}C evolution times can be used to gain high resolution originating from the very sharp carbon lines.

Fig. 7a shows a 2D proton–carbon heteronuclear correlation experiment, recorded on the 800 MHz spectrometer at 60 kHz MAS, which demonstrates the possibility to assign methyl proton chemical shifts, in part due to the reduced number of resonances. Proton line-widths vary from 160 to 300 Hz, which indicates a high variation in the mobility of methyl groups as well as on a possible disorder and heterogeneity of the molecular assembly. The linewidth of the ^{13}C resonances is shown in the ^{13}C projection presented in Supplementary Fig. S3.

In the same conditions as for the 2D spectrum, we recorded a 3D (H)CCH experiment (Fig. 7b) using RFDR [35] to recouple ^{13}C–^{13}C homonuclear dipolar interactions and obtain information about carbon–carbon contacts. Although the RFDR recoupling period lasted moderately long (19.2 ms), we observed only intra-residual contacts as long-range magnetization transfers were suppressed by dipolar truncation [66]. The conducted experiments allowed the assignment of almost all methyl proton signals on the basis of the carbon resonance assignments which were obtained previously [39] and confirmed in Figs. 2e and 5a. The chemical shift of methyl protons can reveal local structural features, such as the shielding and deshielding effects of aromatic rings. As proton chemical shifts are highly sensitive to the surrounding environment, they can also be used as a basis for the comparison of different sample preparations, for instance to detect the binding sites of ligands and to characterize the influence of binding partners. Considering the recent improvements in the performance of chemical shift prediction software packages [67–69], the determination and validation of side-chain conformation could employ side-chain chemical shifts similarly to the present use of backbone chemical shifts.

4. Conclusions

We have reported a straightforward isotopic labeling strategy for the ^{13}C labeling of isoleucine, leucine and valine methyl groups in proteins. For the type-three secretion system needle assembly of MxiH proteins we obtained 10 frequency unambiguous distance restraints, 23 structurally unambiguous distance restraints and 16 ambiguous distance restraints. We could show that the use of the two biosynthetic precursors, sodium α-ketoisovalerate and sodium α-ketobutyrate, is a helpful tool to achieve clear and ultra-sparsely labeled ^{13}C methyl group spectra, with a high resolution for ^{13}C resonances (line-widths as low as 22.2 Hz; see Supplementary Fig. S3). We demonstrated the possibility of recording NCX spectra where long-range distance correlations were detected. As well, the high resolution of peaks and the spectral simplification enabled many important applications for the study of proteins: the assignment of methyl proton chemical shifts, the collection of long-range restraints, and the study of dynamics. The proposed labeling strategy can be employed to advance the study of large and complex protein systems.

Acknowledgments

We thank Brigitta Angerstein for expert technical help. This work was supported by the Max Planck Society, the Leibniz-Institut für Molekulare Pharmakologie, the Deutsche Forschungsgemeinschaft (Emmy Noether Fellowship to A. Lange), the NSERC of Canada (Postgraduate Scholarship to J.P.D.) and the European Union Seventh Framework Program under Grant Agreement 261863 (Bio-NMR).

Appendix A. Supplementary material

Supplementary data associated with this article can be found, in the online version, at http://dx.doi.org/10.1016/j.jmr.2014.12.013.

References

[1] R. Tycko, Solid-state NMR studies of amyloid fibril structure, in: S.R. Leone, P.S. Cremer, J.T. Groves, M.A. Johnson (Eds.), Annual Review of Physical Chemistry, 2011, pp. 279–299.
[2] J.C.C. Chan, Solid-state NMR techniques for the structural determination of amyloid fibrils, in: J.C.C. Chan (Ed.) Solid State Nuclear Magnetic Resonance, 2012, pp. 47–88.
[3] G. Comellas, C.M. Rienstra, Protein structure determination by magic-angle spinning solid-state NMR, and insights into the formation, structure, and stability of amyloid fibrils, in: K.A. Dill (Ed.) Ann. Rev. Biophys., 2013, pp. 515–536.
[4] R. Tycko, R.B. Wickner, Molecular structures of amyloid and prion fibrils: consensus versus controversy, Acc. Chem. Res. 46 (2013) 1487–1496.
[5] A. McDermott, Structure and dynamics of membrane proteins by magic angle spinning solid-state NMR, Ann. Rev. Biophys. 38 (2009) 385–403.
[6] M. Hong, Y. Zhang, F.H. Hu, Membrane protein structure and dynamics from NMR spectroscopy, in: Annual Review of Physical Chemistry, Annual Reviews, Palo Alto, 2012, pp. 1–24.
[7] W.T. Franks, A.H. Linden, B. Kunert, B.J. van Rossum, H. Oschkinat, Solid-state magic-angle spinning NMR of membrane proteins and protein-ligand interactions, Eur. J. Cell Biol. 91 (2012) 340–348.
[8] S. Sun, Y. Han, S. Paramasivam, S. Yan, A.E. Siglin, J.C. Williams, I.-J.L. Byeon, J. Ahn, A.M. Gronenborn, T. Polenova, Solid-state NMR spectroscopy of protein complexes, in: A. Shekhtman, D.S. Burz (Eds.) Protein NMR Techniques, third ed., 2012, pp. 303–331.
[9] A. Goldbourt, Biomolecular magic-angle spinning solid-state NMR: recent methods and applications, Curr. Opin. Biotech. 24 (2013) 705–715.
[10] A. Loquet, B. Habenstein, J.-P. Demers, S. Becker, A. Lange, Structure of a bacterial nanomachine type 3 secretion system needle, Med. Sci.: M/S 28 (2012) 926–928.
[11] A. Loquet, B. Habenstein, A. Lange, Structural investigations of molecular machines by solid-state NMR, Acc. Chem. Res. 46 (2013) 2070–2079.
[12] D. Huster, Solid-state NMR studies of collagen structure and dynamics in isolated fibrils and in biological tissues, in: G.A. Webb (Ed.) Annual Reports on NMR Spectroscopy, 2008, pp. 127–159.
[13] A.A. Arnold, I. Marcotte, Studying natural structural protein fibers by solid-state nuclear magnetic resonance, Concepts Magn. Reson. Part A 34A (2009) 24–47.
[14] D. Laurencin, A. Wong, W. Chrzanowski, J.C. Knowles, D. Qiu, D.M. Pickup, R.J. Newport, Z.H. Gan, M.J. Duer, M.E. Smith, Probing the calcium and sodium local environment in bones and teeth using multinuclear solid state NMR and X-ray absorption spectroscopy, Phys. Chem. Chem. Phys. 12 (2010) 1081–1091.
[15] J.-P. Demers, V. Chevelkov, A. Lange, Progress in correlation spectroscopy at ultra-fast magic-angle spinning: basic building blocks and complex experiments for the study of protein structure and dynamics, Solid State Nucl. Mag. Reson. 40 (2011) 101–113.
[16] A. Lange, K. Seidel, L. Verdier, S. Luca, M. Baldus, Analysis of proton-proton transfer dynamics in rotating solids and their use for 3D structure determination, J. Am. Chem. Soc. 125 (2003) 12640–12648.
[17] A. Lange, S. Becker, K. Seidel, K. Giller, O. Pongs, M. Baldus, A concept for rapid protein-structure determination by solid-state NMR spectroscopy, Angew. Chem. 44 (2005) 2089–2092.
[18] D. Suter, R. Ernst, Spin diffusion in resolved solid-state NMR spectra, Phys. Rev. B 32 (1985) 5608–5627.
[19] N.M. Szeverenyi, M.J. Sullivan, G.E. Maciel, Observation of spin exchange by two-dimensional fourier-transform 13C cross polarization-magic-angle spinning, J. Magn. Reson. 47 (1982) 462–475.
[20] K. Takegoshi, S. Nakamura, T. Terao, ^{13}C–^{1}H dipolar-assisted rotational resonance in magic-angle spinning NMR, Chem. Phys. Lett. 344 (2001) 631–637.
[21] C.R. Morcombe, V. Gaponenko, R.A. Byrd, K.W. Zilm, Diluting abundant spins by isotope edited radio frequency field assisted diffusion, J. Am. Chem. Soc. 126 (2004) 7196–7197.
[22] G. De Paepe, J.R. Lewandowski, A. Loquet, A. Bockmann, R.G. Griffin, Proton assisted recoupling and protein structure determination, J. Chem. Phys. 129 (2008) 245101.
[23] J.R. Lewandowski, G. De Paepe, R.G. Griffin, Proton assisted insensitive nuclei cross polarization, J. Am. Chem. Soc. 129 (2007) 728–729.
[24] T. Gullion, J. Schaefer, Rotational-echo double-resonance NMR, J. Magn. Reson. 81 (1989) 196–200.
[25] A.W. Hing, S. Vega, J. Schaefer, Transferred-echo double-resonance NMR, J. Magn. Reson. 96 (1992) 205–209.
[26] F. Castellani, B. van Rossum, A. Diehl, M. Schubert, K. Rehbein, H. Oschkinat, Structure of a protein determined by solid-state magic-angle-spinning NMR spectroscopy, Nature 420 (2002) 98–102.
[27] M. Hong, K. Jakes, Selective and extensive ^{13}C labeling of a membrane protein for solid-state NMR investigations, J. Biomol. NMR 14 (1999) 71–74.
[28] A. Loquet, B. Habenstein, V. Chevelkov, S.K. Vasa, K. Giller, S. Becker, A. Lange, Atomic structure and handedness of the building block of a biological assembly, J. Am. Chem. Soc. 135 (2013) 19135–19138.
[29] D.M. LeMaster, D.M. Kushlan, Dynamical mapping of *E-coli* thioredoxin via C-13 NMR relaxation analysis, J. Am. Chem. Soc. 118 (1996) 9255–9264.
[30] M. Hong, Determination of multiple phi-torsion angles in proteins by selective and extensive C-13 labeling and two-dimensional solid-state NMR, J. Magn. Reson. 139 (1999) 389–401.
[31] A. Loquet, K. Giller, S. Becker, A. Lange, Supramolecular interactions probed by ^{13}C–^{13}C solid-state NMR spectroscopy, J. Am. Chem. Soc. 132 (2010) 15164–15166.
[32] A. Loquet, G. Lv, K. Giller, S. Becker, A. Lange, ^{13}C spin dilution for simplified and complete solid-state NMR resonance assignment of insoluble biological assemblies, J. Am. Chem. Soc. 133 (2011) 4722–4725.
[33] M.T. Eddy, M. Belenky, A.C. Sivertsen, R.G. Griffin, J. Herzfeld, Selectively dispersed isotope labeling for protein structure determination by magic angle spinning NMR, J. Biomol. NMR 57 (2013) 129–139.
[34] C. Guo, C. Geng, V. Tugarinov, Selective backbone labeling of proteins using 1,2-^{13}C2-pyruvate as carbon source, J. Biomol. NMR 44 (2009) 167–173.
[35] A.E. Bennett, R.G. Griffin, J.H. Ok, S. Vega, Chemical shift correlation spectroscopy in rotating solids: radio frequency-driven dipolar recoupling and longitudinal exchange, J. Chem. Phys. 96 (1992) 8624–8627.
[36] D.K. Sodickson, M.H. Levitt, S. Vega, R.G. Griffin, Broad-band dipolar recoupling in the nuclear-magnetic-resonance of rotating solids, J. Chem. Phys. 98 (1993) 6742–6748.
[37] M.J. Bayro, T. Maly, N.R. Birkett, C.M. Dobson, R.G. Griffin, Long-range correlations between aliphatic ^{13}C nuclei in protein MAS NMR spectroscopy, Angew. Chem.-Int. Edit. 48 (2009) 5708–5710.
[38] A. Loquet, N.G. Sgourakis, R. Gupta, K. Giller, D. Riedel, C. Goosmann, C. Griesinger, M. Kolbe, D. Baker, S. Becker, A. Lange, Atomic model of the type III secretion system needle (vol. 486, p. 276, 2012), Nature 488 (2012).
[39] J.-P. Demers, N.G. Sgourakis, R. Gupta, A. Loquet, K. Giller, D. Riedel, B. Laube, M. Kolbe, D. Baker, S. Becker, A. Lange, The common structural architecture of *Shigella flexneri* and *Salmonella typhimurium* type three secretion needles, Plos Pathogens 9 (2013) e1003245.
[40] G. Lv, H.K. Fasshuber, A. Loquet, J.P. Demers, V. Vijayan, K. Giller, S. Becker, A. Lange, A straightforward method for stereospecific assignment of val and leu prochiral methyl groups by solid-state NMR: scrambling in the [2-^{13}C]Glucose labeling scheme, J. Magn. Reson. 228 (2013) 45–49.
[41] B. Habenstein, A. Loquet, K. Giller, S. Becker, A. Lange, Structural characterization of supramolecular assemblies by ^{13}C spin dilution and 3D solid-state NMR, J. Biomol. NMR 55 (2013) 1–9.
[42] V. Tugarinov, P.M. Hwang, L.E. Kay, Nuclear magnetic resonance spectroscopy of high-molecular-weight proteins, Ann. Rev. Biochem. 73 (2004) 107–146.
[43] I. Gelis, A.M.J.J. Bonvin, D. Keramisanou, M. Koukaki, G. Gouridis, S. Karamanou, A. Economou, C.G. Kalodimos, Structural basis for signal-sequence recognition by the translocase motor SecA as determined by NMR, Cell 131 (2007) 756–769.
[44] T.M. Sabo, D. Bakhtiari, K.F.A. Walter, R.L. McFeeters, K. Giller, S. Becker, C. Griesinger, D. Lee, Thermal coefficients of the methyl groups within ubiquitin, Protein Sci. 21 (2012) 562–570.
[45] M. Bista, S.M. Freund, A.R. Fersht, Domain-domain interactions in full-length p53 and a specific DNA complex probed by methyl NMR spectroscopy, Proc. Natl. Acad. Sci. U.S.A. 109 (2012) 15752–15756.
[46] M. Huber, S. Hiller, P. Schanda, M. Ernst, A. Bockmann, R. Verel, B.H. Meier, A proton-detected 4D solid-state NMR experiment for protein structure determination, Chemphyschem: Eur. J. Chem. Phys. Phys. Chem. 12 (2011) 915–918.
[47] P.J. Hajduk, D.J. Augeri, J. Mack, R. Mendoza, J.G. Yang, S.F. Betz, S.W. Fesik, NMR-based screening of proteins containing C-13-labeled methyl groups, J. Am. Chem. Soc. 122 (2000) 7898–7904.
[48] C.R. Morcombe, K.W. Zilm, Chemical shift referencing in MAS solid state NMR, J. Magn. Reson. 162 (2003) 479–486.
[49] T.D. Goddard, D.G. Kneller, SPARKY 3, in: S.F. University of California (Ed.), 2006.
[50] M. Baldus, D.G. Geurts, S. Hediger, B.H. Meier, Efficient ^{15}N–^{13}C polarization transfer by adiabatic-passage Hartmann–Hahn cross polarization, J. Magn. Reson. Ser. A 118 (1996) 140–144.

[51] M. Baldus, A.T. Petkova, J. Herzfeld, R.G. Griffin, Cross polarization in the tilted frame: assignment and spectral simplification in heteronuclear spin systems, Mol. Phys. 95 (1998) 1197–1207.
[52] D.H. Zhou, C.M. Rienstra, High-performance solvent suppression for proton detected solid-state NMR, J. Magn. Reson. 192 (2008) 167–172.
[53] A. Detken, E.H. Hardy, M. Ernst, B.H. Meier, Simple and efficient decoupling in magic-angle spinning solid-state NMR: the XiX scheme, Chem. Phys. Lett. 356 (2002) 298–304.
[54] A.J. Shaka, J. Keeler, T. Frenkiel, R. Freeman, An improved sequence for broadband decoupling: WALTZ-16, J. Magn. Reson. 52 (1983) 335–338.
[55] D. Neri, T. Szyperski, G. Otting, H. Senn, K. Wuthrich, Stereospecific nuclear magnetic-resonance assignments of the methyl-groups of valine and leucine in the DNA-binding domain of the 434-repressor by biosynthetically directed fractional ^{13}C labeling, Biochemistry 28 (1989) 7510–7516.
[56] R.J. Lichtenecker, K. Weinhaeupl, L. Reuther, J. Schoerghuber, W. Schmid, R. Konrat, Independent valine and leucine isotope labeling in *Escherichia coli* protein overexpression systems, J. Biomol. NMR 57 (2013) 205–209.
[57] R.J. Lichtenecker, K. Weinhaeupl, W. Schmid, R. Konrat, Alpha-Ketoacids as precursors for phenylalanine and tyrosine labelling in cell-based protein overexpression, J. Biomol. NMR 57 (2013) 327–331.
[58] D.F. Hansen, L.E. Kay, Determining valine side-chain rotamer conformations in proteins from methyl C-13 chemical shifts: application to the 360 kDa half-proteasome, J. Am. Chem. Soc. 133 (2011) 8272–8281.
[59] P. Fricke, J.-P. Demers, S. Becker, A. Lange, Studies on the MxiH protein in T3SS needles using DNP-enhanced ssNMR spectroscopy, Chemphyschem: Eur. J. Chem. Phys. Phys. Chem. 15 (2014) 57–60.
[60] M. Nilges, M.J. Macias, S.I. Odonoghue, H. Oschkinat, Automated NOESY interpretation with ambiguous distance restraints: the refined NMR solution structure of the pleckstrin homology domain from beta-spectrin, J. Mol. Biol. 269 (1997) 408–422.
[61] M. Fossi, T. Castellani, M. Nilges, H. Oschkinat, B.J. van Rossum, SOLARIA: a protocol for automated cross-peak assignment and structure calculation for solid-state magic-angle spinning NMR spectroscopy, Angew. Chem.-Int. Ed. 44 (2005) 6151–6154.
[62] S.A. Shahid, B. Bardiaux, W.T. Franks, L. Krabben, M. Habeck, B.-J. van Rossum, D. Linke, Membrane-protein structure determination by solid-state NMR spectroscopy of microcrystals, Nature Methods 9 (2012). 1212-U1119.
[63] J.P. Demers, B. Habenstein, A. Loquet, S. Kumar Vasa, K. Giller, S. Becker, D. Baker, A. Lange, N.G. Sgourakis, High-resolution structure of the Shigella type-III secretion needle by solid-state NMR and cryo-electron microscopy, Nature Commun. 5 (2014) 4976.
[64] P. Guntert, Automated structure determination from NMR spectra, Eur. Biophys. J. Biophys. Lett. 38 (2009) 129–143.
[65] D.H. Zhou, G. Shah, M. Cormos, C. Mullen, D. Sandoz, C.M. Rienstra, Proton-detected solid-state NMR spectroscopy of fully protonated proteins at 40 kHz magic-angle spinning, J. Am. Chem. Soc. 129 (2007) 11791–11801.
[66] P. Hodgkinson, L. Emsley, The accuracy of distance measurements in solid-state NMR, J. Magn. Reson. 139 (1999) 46–59.
[67] H. Beomsoo, L. Yifeng, S.W. Ginzinger, D.S. Wishart, SHIFTX2: significantly improved protein chemical shift prediction, J. Biomol. NMR 50 (2011) 43–57.
[68] J. Meiler, PROSHIFT: protein chemical shift prediction using artificial neural networks, J. Biomol. NMR 26 (2003) 25–37.
[69] P.R. Rablen, S.A. Pearlman, J. Finkbiner, A comparison of density functional methods for the estimation of proton chemical shifts with chemical accuracy, J. Phys. Chem. A 103 (1999) 7357–7363.